GEOMECHANICAL MODELLING OF FRACTURING AND DAMAGE INDUCED BY IGNEOUS INTRUSIONS: IMPLICATIONS FOR FLUID FLOW IN VOLCANIC BASINS

Olivier Galland[1], Tobias Schmiedel[1], Håvard Bertelsen[1], Frank Guldstrand[1], Øystein T. Haug[1], Alban Souche[1]

1: Physics of Geological Processes, the NJORD Center, University of Oslo, Norway,
olivier.galland@geo.uio.no, tobias.schmiedel@geo.uio.no, h.s.bertelsen@geo.uio.no,
f.b.b.guldstrand@geo.uio.no, oystein.t.haug@gmail.com, alban.souche@geo.uio.no,

Keywords: **sills, laccoliths, geomechanical modelling, fractures, structural traps**

RESUMEN

La última década de investigación muestro que muchas cuencas sedimentarias en el mundo contienen voluminosos complejos ígneos intrusivos, sobre todo filones capas y lacolitos. Estas intrusiones ígneas tienen enormes implicaciones en el sistema petrolero a través de la maduración, la circulación y la trampa de hidrocarburos. En esta contribución, nos centramos en las implicaciones estructurales y mecánicas de las intrusiones ígneas en las rocas cajas sedimentarias. Cuando el magma se introduce en las rocas sedimentarias, hace su espacio empujando y rompiendo la roca caja, lo que puede ocasionar daños intensos y fracturas. Comprender y cuantificar la distribución de dicho patrón de deformación inelástica inducida por intrusión es esencial para restringir adecuadamente las vías de migración de hidrocarburos y las trampas alrededor de filones capas y lacolitos. Sin embargo, la mayoría de los modelos establecidos de emplazamiento de filones capas y lacolitos solo dan cuenta de las rocas elásticas que se rompen en tensión, por lo que no pueden predecir la distribución de fracturas y daños inelástico alrededor de las intrusiones ígneas. En la Universidad de Oslo, diseñamos un conjunto novedoso de métodos de modelamiento para estudiar y cuantificar el emplazamiento del magma y las fracturas y distribución del daño asociadas. En este documento, desarrollamos una compilación resumida de estos métodos: experimentos de laboratorio 3D, experimentos de laboratorio 2D y modelos numéricos. Los resultados de nuestros modelos destacan la importante contribución de la deformación inelástica de la roca caja de los filónes capas, donde un daño de cizallamiento inelástico sustancial y fallamiento puede desarrollarse. En general, nuestros modelos muestran que los modelos establecidos de emplazamiento de filones capas y lacolitos, basados en la suposición de que la roca madre se deforma por flexión elástica, son limitados y que las propiedades frágiles de Coulomb de las rocas sedimentarias deben tenerse en cuenta para entender la naturaleza y distribución de las fracturas y daño asociado con intrusiones ígneas.

INTRODUCTION

Seismic reflection data have over the past few decades revealed the presence of voluminous igneous complexes in sedimentary basins, such as the Neuquén Basin (Spacapan *et al.* 2017;

Rabbel *et al.* 2018; Spacapan *et al.* 2018). Igneous intrusions in these basins exhibit various shapes, from flat sills, saucer-shaped sills, to laccoliths (Galland *et al.* 2018). It has been demonstrated that intrusive rocks and processes have major impacts on the thermal and structural evolutions of petroleum systems (Petford and McCaffrey 2003; Schutter 2003; Senger *et al.* 2017):

- Sills are emplaced along preferential stratigraphic levels such as organic-rich shale, where the heat provided by the magma locally maturates the organic matter in the surrounding sediments (Rodriguez Monreal *et al.* 2009; Aarnes *et al.* 2011; Spacapan *et al.* 2018).
- Injection of high-pressure magma may cause uplift and deformation of the host rock, forming broad domes (Figure 1), or "forced folds", of their overlaying strata (e.g., Trude *et al.* 2003; Jackson *et al.* 2013; Magee *et al.* 2013), some of which represent hydrocarbon traps (Orchuela *et al.* 2003; Schmiedel *et al.* 2017b).
- The damage induced by the emplacement of magma in the host rock produce numerous fractures enhancing fluid flow (Delaney and Pollard 1981; Chevallier *et al.* 2004; Senger *et al.* 2015).
- Igneous intrusions are heavily fractured due to cooling effects, and they represent highly productive hydrocarbon reservoirs (Rodriguez Monreal *et al.* 2009; Witte *et al.* 2012) and migration conduits for hydrocarbons (Rateau *et al.* 2013).
- Igneous intrusions also represent potential problems for hydrocarbon exploration and production, such as compartmentalization, drilling issues and overpressure cages.

These effects highlight qualitatively that an in-depth understanding of the overall processes associated with the emplacement of igneous intrusions in sedimentary basins is essential for robust understanding of the petroleum system in volcanic basins. In this paper, we will focus on the mechanics of magma emplacement and their structural implications at both large-scale (forced folds) and small-scale (damage) structures. We designed a new suite of analogue and numerical geomechanical modelling tools to reveal the inelastic structures in the host rock that accommodate the emplacement of sills and laccoliths. We will describe the modelling methodologies and characteristic results of (1) 3D laboratory models, (2) 2D laboratory models, and (3) numerical models. Finally, we will discuss the relevance of our novel models with respect to established models.

3D LABORATORY MODELS

Experimental method

The 3D experimental method used in this study is similar to that presented by Schmiedel *et al.* (2017a). The model rock and model magma consist of dry Mohr-Coulomb granular materials of variable cohesion, i.e. shear strength (Galland *et al.* 2006; Abdelmalak *et al.* 2016), and molten

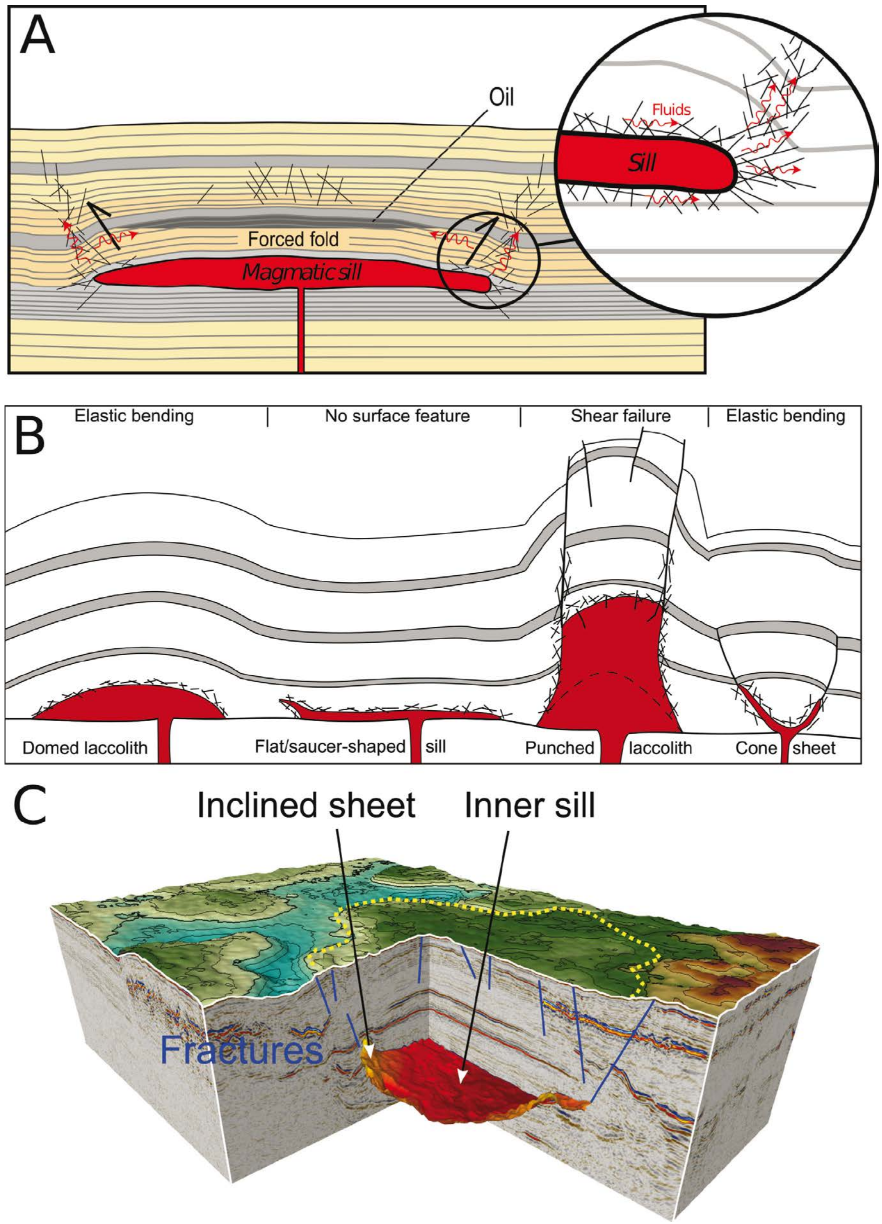

Figure 1. Examples illustrating the structural implications of igneous intrusions on their host rock. A. Schematic drawing of igneous sill and mechanical implications on sedimentary host rock. Intrusion-scale doming, or forced folds, can be hydrocarbon traps, whereas small-scale fractures and damage can be fluid pathways. B. Schematic drawing of various degrees of overburden deformation associated thin sills, domes laccoliths and punched laccoliths. Modified from Delpino *et al.* (2014). C. 3D seismic block of the Tulipan sill and the associated structures in its overburden, Møre Basin, offshore Norway. From Schmiedel *et al.* (2017b).

vegetable oil, respectively (Figure 2). The granular materials used in this study consist of a mix of (1) a high cohesion fine-grained crystalline silica flour (SF; cohesion of ~600 Pa), and (2) a low cohesion micro glass beads (GB; cohesion of ~100 Pa; Figure 2). These granular mixtures simulate a wide range of brittle rocks, from strong, competent rocks (e.g. limestone) to weak rocks (e.g. shale). The molten vegetable oil has a viscosity of $\eta = 2 \times 10^{-2}$ Pa s at 50°C (Galland *et al.* 2006). Schmiedel *et al.* (2017a) and Guldstrand *et al.* (2017b) discussed that the oil is suitable for simulating magmas of intermediate to high viscosity in nature, i.e. those found in the Neuquén

Basin. The relevance of these materials and the scaling of the models are described in detail by Galland *et al.* (2014) and Schmiedel *et al.* (2017a), and references therein.

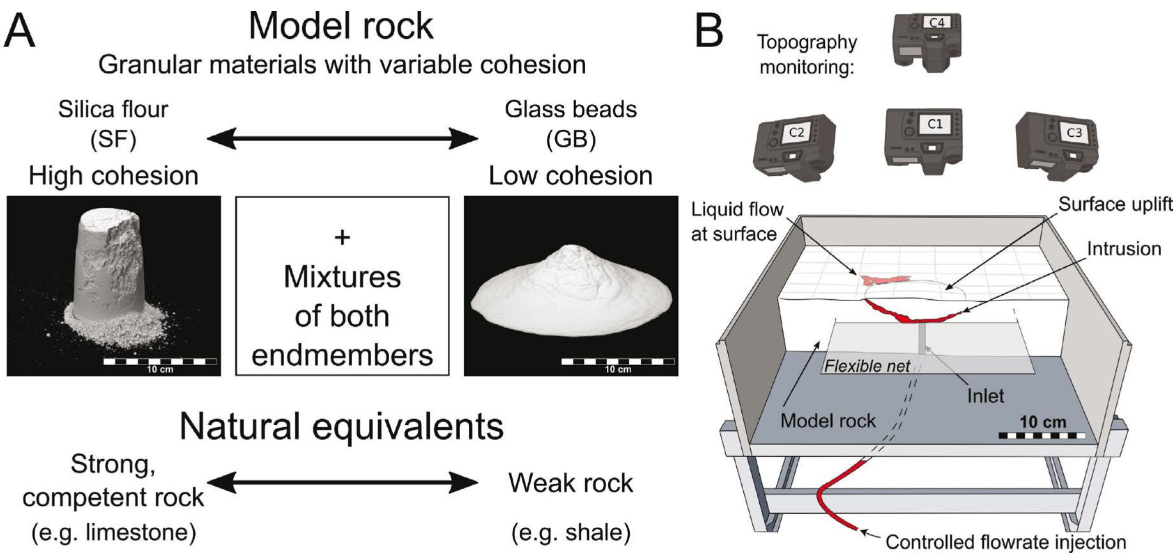

Figure 2. a. Photographs of granular materials used to model brittle rocks. Left: high cohesion, fine-grained crystaline silica flour to model competent rocks. Right: low cohesion, fine-grained glass beads to model loose rocks. B. Drawing of the 3D experimental setup to model magma emplacement in the brittle crust. Four synchronized cameras monitor the evolution of the model surface.

Figure 2B shows a sketch of the experimental setup. We prepared the experiments by compacting two layers of the same granular material in a 0.4 x 0.4 m box (Figure 2B) using a high frequency compressed-air shaker (Houston Vibrator model GT-25). The compaction procedure was conducted as follows: (1) we poured a first layer of granular material of known mass in the box and gently compacted it, (2) we placed a flexible net on top of the compacted lower layer to simulate a thin horizontal layer or strata, (3) we poured a second mass of the same Coulomb granular material and we compacted the whole model. We controlled the amount of compaction such that (1) the net was located just in contact with the injection inlet, and (2) the density of the upper layer, and so the thickness of the upper layer, was known with great precision. We estimate the density difference between the two layers of compacted granular materials to be <5%. This compaction procedure allows for a good reproducibility of the granular material density (uncertainty < 5%), and therefore a good control of the cohesion (Galland *et al.* 2009). We assume the flexible net in our laboratory models is a valid approximation to simulate a weak interface between sedimentary layers in nature, given that the strength contrasts in layered rocks can be as high as several orders of magnitude (Schellart 2000; Schmiedel *et al.* 2017a). However, the mechanical effect of the flexible net is hard to quantify.

In our experiments we injected the model magma (vegetable oil) with a constant volumetric flow rate Q of 40 ml min-1 (= 5.1 x 10^{-7} m^3 s^{-1}). Because the net is located just at the inlet (Figure 2B), the oil directly flows horizontally along the flexible net to form a sill before propagating upwards. Thus, our experiments do not consider the feeder-to-sill transition. In all experiments, the horizontal extent of the flexible net was significantly larger than the final intrusion diameters, therefore boundary effects on the oil propagation due to the flexible net are negligible.

During the experiments, we monitored the surface deformation induced by the intruding oil using a photogrammetry system based on four synchronized cameras (Figure 2B) (Galland *et al.* 2016; Schmiedel *et al.* 2017a). This photogrammetry system captured the model surface with a frequency of 1Hz and produced high-resolution (< 0.1 mm) and high-precision (~0.05 mm) topographic maps (Galland *et al.* 2016; Schmiedel *et al.* 2017a). In addition, advanced digital image correlation (DIC) function allows high-precision (< 0.1 mm) and high-resolution calculation of horizontal displacements on the model surface (Galland *et al.* 2016). After the end of each experiment, the oil solidified, we carefully excavated the intrusions in situ and we digitalized their 3D shapes using photogrammetry (Galland *et al.* 2016; Schmiedel *et al.* 2017a) (Figure 3). This procedure allows a direct comparison between the intrusion geometry and the associated surface deformation.

Results

We observe variable intrusion geometries with respect to the experimental parameters. In high cohesion experiments, the intrusions were typical saucer-shaped, with circular, flat, horizontal inner sill and outer inclined sheets (Figure 3, top). In contrast, in low cohesion experiments, the intrusions were massive, piston-like intrusions, with sub-vertical sidewalls (Figure 3, bottom). Finally, in experiments with intermediate cohesions, the intrusions exhibit mostly inclined sheets, with a sub-horizontal bottom intrusion of radius smaller than those of intrusions emplaced in the high-cohesion experiments (Schmiedel *et al.* 2017a). The sheets in intermediate-cohesion experiments appear thicker than those in the high-cohesion experiments.

The surface deformation in the high-cohesion experiments shows a smooth dome structure with small h/w values (dome height h/dome diameter w) and small surface curvatures (Figure 3, top). Additionally, orthorectified images of the model surfaces display small tensile fractures, which concentrate in the areas of the dome with the highest curvature (Figure 4). In low cohesion experiments, the model surface develops drastically distinct and discontinuous features (Figure 3, bottom; Schmiedel *et al.* 2017a): (1) intrusions trigger the formation of circular dome structures with a large h/w value; (2) the outer boundary of the dome is sharp, (3) the domes exhibit blocky structures, the individual blocks being separated by dominantly shear fractures (i.e. faults). Finally, in intermediate cohesion experiments, the model surface deformation patterns exhibit domes that combine characteristics of those of high- and low-cohesion experiments (Schmiedel *et al.* 2017a). The domes were not blocky, but the values of h/w and the curvatures of the domes were higher than those of high-cohesion experiments. We will discuss the scaling of h/w later (see also supplemental material).

An important aspect of the trapping properties of forced folds induced by igneous sills and laccoliths is fracture development (Figure 4A). Visual observation on orthorectified images of the model surfaces highlights the formation of surface discontinuities, i.e. fractures (Figure 4B). In the middle of the uplifted area, a few open, dilating cracks are clearly visible, while at the edges of the uplifted area fractures accommodating shortening are visible (Figure 4B). Such a fracture pattern is compatible with stress distribution across a dome induced by a shallow intrusion (e.g. Pollard and Johnson 1973; Galland and Scheibert 2013). Displacement maps calculated automatically from DIC analysis highlight clear discontinuities (Galland *et al.* 2016) coinciding with the visible surface fractures. A simple method to highlight surface fractures is to compute the divergence and the shear strain fields from the displacement maps using e.g. straightforward Matlab® scripts. Figure 4C displays time series of divergence maps computed from the displacement maps of a characteristic experiment. They clearly highlight the presence of numerous cracks, the majority of which are too small to be visually observed on the orthorectified image of Figure 4B. The divergence field nicely images opening cracks (positive divergence) in the uplifted area and the shortening fractures (negative divergence) at the edge of the uplifted area.

The periodic monitoring of the experiments allows one to analyze the evolution of the model surfaces by highlighting incremental deformation (Figure 4D). Early in the experiments (Figure 4D, left), the uplifted area has a symmetrical shape, and the divergence plot indicates dilation, i.e. open tensile fractures in a radial pattern. In the later stages (Figure 4D, centre and right), however, a clear asymmetry develops: the point of maximum uplift move to the left. The tensile fracture pattern shown on the divergence plot also gradually changes from a radial pattern to a dominantly circumferential pattern.

TWO-DIMENSIONAL LABORATORY MODELS

Method

Even if the 3D experiments provide excellent mechanical understanding of the large-scale deformation induced by igneous intrusions, the opaque granular materials used in these experiments do not allow us to observe the local subsurface damage induced by the emplacement and propagation of the intrusions. To overcome this limitation, we designed 2D laboratory experiments.

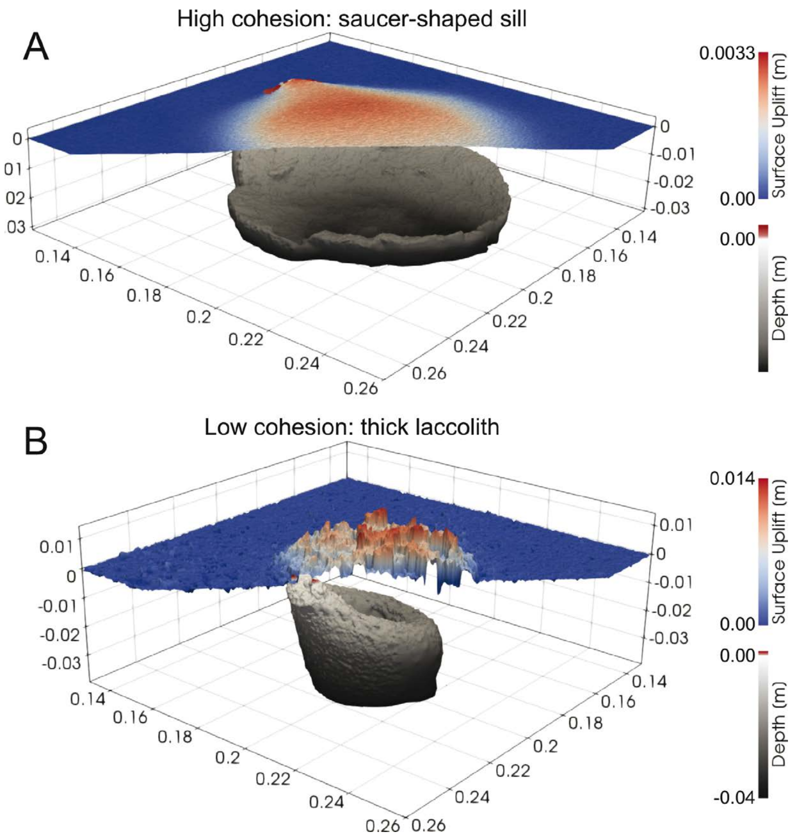

Figure 3. A. Block diagram plotting digital elevation model (DEM) (colour) of model surface and underlying saucer-shaped intrusion from a characteristic 3D experiment in a high-cohesion experiment. The DEM evidences low amplitude, smooth uplift above the intrusion. B. Block diagram plotting digital elevation model (DEM) (colour) of model surface and underlying saucer-shaped intrusion from a characteristic 3D experiment in a low-cohesion experiment. The DEM evidences high amplitude, blocky uplift above the intrusion.

The experimental setup is designed after that of Abdelmalak *et al.* (2012) but also includes improvements to the compaction system and inlet design. The rock analogues are the same dry granular materials as those used in the 3D experiments. The magma analogue was Golden Syrup. The viscosity of Golden syrup is highly temperature dependent, which is why we injected it at a constant room temperature of ~ 21°C at which the viscosity is ~55 Pa s and a density of ~1440 kg m^{-3}.

The experimental setup consists of a thick 2D hele-shaw cell with dimensions 80 cm wide, 50 cm high and 3 cm thick (Figure 5). The preparation procedure of the granular materials was the same as that in the 3D experiments. An interchangeable inlet is placed at the bottom of the cell to inject the Golden Syrup. The viscous golden syrup was put into a syringe and allowed to degas during host rock preparation. The syringe was then put into the syringe pump and connected to the inlet with a T-connector in-between pump and inlet where pressure readings were taken using a pressure sensor and Arduino system. The experiments were done at constant flow rate for all experiments of 0.5 ml min-1 resulting in experiment durations of ~52-130 min.

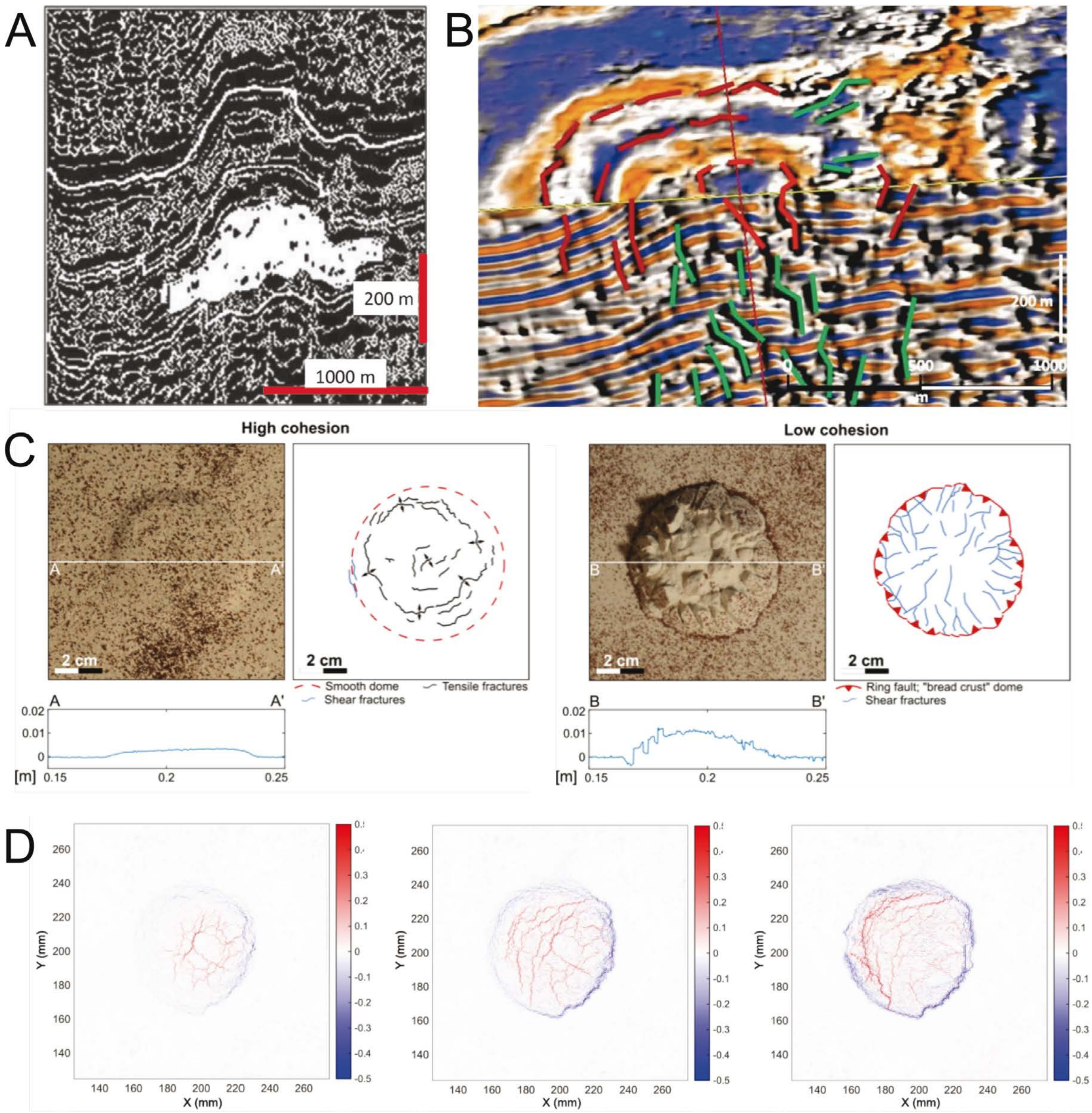

Figure 4. A. Seismic data of an igneous laccolith (white) and doming of the overburden layers in the southern Mendoza Province, Neuquén Basin (Delpino *et al*. 2014). B. 3D seismic block of interpreted deformed overburden of a laccolith, in the southern Mendoza Province, Argentina (Delpino *et al*. 2014). Deformation exhibits doming and fracturing. C. Left: orthorectified image, interpreted structural drawing of the image, and topographic profile of the surface of an experiment with high cohesion granular material. Note the numerous tensile fractures. Right: orthorectified image, interpreted structural drawing of the image, and topographic profile of the surface of an experiment with low cohesion granular material. Note the numerous shear fractures (faults). After Schmiedel *et al*. (in review). D. Time series divergence maps of the surface of a characteristic experiment. Red lines mark tensile fractures (positive divergence) while blue lines mark compressional fractures (negative divergence). After Galland *et al*. (2016).

The emplacement of the Golden Syrup in the models was observable from the sides through the glass plates, and monitored using a DSLR camera. We applied digital image correlation between successive images to compute the displacements of the host that accommodate the propagating

Golden Syrup. We subsequently calculate divergence and shear strain maps to highlight the development of small-scale subsurface structures associated with the propagation of the Golden Syrup (Figure 6).

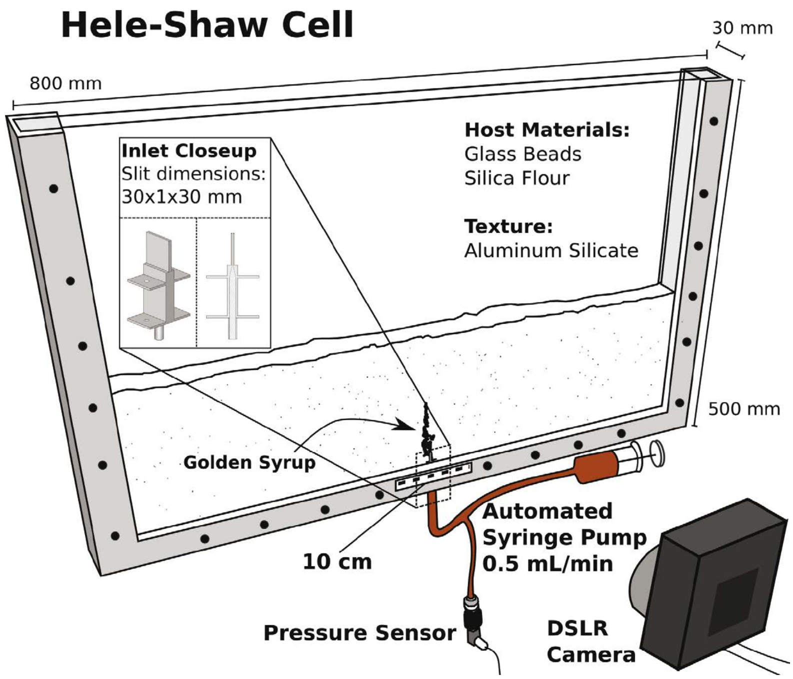

Figure 5. Drawing of the 2D experimental setup to model magma emplacement in the brittle crust.

Results

In these experiments, we modeled the development of subvertical dykes, which occurred in two stages. During Stage 1, the propagation of a vertical dyke triggered gentle surface uplift spread over a large area (Figure 6), and open cracks affecting the surface. Stage 2 initiates when the initial vertical dyke reached 5–6 cm below the surface (Figure 6), it sharply bent to horizontal, and subsequently bent to sub-vertical by following the traces of open cracks formed during stage 1. When this sharp transition occurred, the surface uplift accelerated (Figure 6). The uplift became suddenly restricted to a very narrow area, bounded by sub-vertical walls. Photographs of Figure 6 show that this uplift is associated with the upward movement of the block of flour delimited by the two main open cracks formed during stage 1, i.e. a popup structure.

The displacement and strain calculations provide essential dynamic and structural information of the development of the intrusion. During Stage 1, the initial vertical dyke produced horizontal displacements on each side of the dyke, indicating opening and enlargement of the intrusion (Figure 6). During upward propagation of the dyke, horizontal displacements mostly occurred close to the upper tip of the dyke and became negligible at its base. Small amplitude upward movements affected a broad symmetrical conical area of the overburden of the dyke, with diffuse boundaries. This uplifted area became narrower as the dyke propagated upward. In this initial stage, shear strain in the model is limited, except for a local V-shaped deformation pattern in the vicinity of the dyke tip (Figure 6). When the dyke reached 7 cm below the surface, important shear deformation occurred between the tip of the dyke and the model surface, while the dyke remained vertical. This is evidenced by the sharp boundaries in the vertical displacement field, indicating that the upward displacement of the overburden was accommodated by two conjugate reverse shear zones. These shear bands are the downward continuation of the open fractures that affected the model surface.

Stage 2 started when the dyke tip intersected one of the shear zones formed at the end of stage 1 (Figure 6). The upward movements of the overburden became strictly restricted to a small domain bounded by the two reverse shear zones formed at the end of stage 1, isolating a

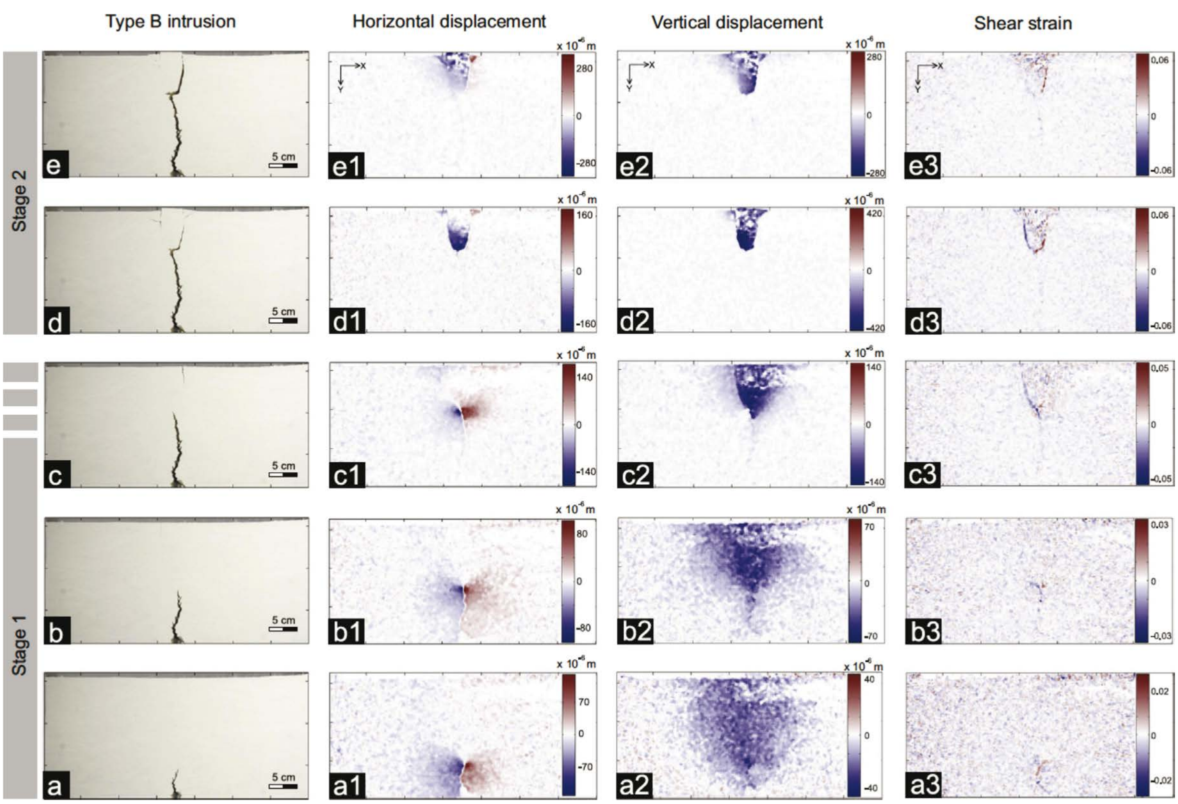

Figure 6. Time-lapse photographs (left column), vertical maps of horizontal displacement (second left column), vertical displacements (third left column) and shear strains (right column) of an experiment of dyke emplacement. From Abdelmalak *et al.* (2012).

"popup" structure (Figure 6). The size of this popup structure remained constant during stage 2. After a sharp bending, the dyke tip followed the trajectory of one of the reverse shear bands. In the shallowest centimetre of the model, additional reverse faults formed on each side of the popup.

These preliminary experiments address the emplacement of dykes, i.e. intrusions of simple geometry. These experiments can be easily adapted to model the emplacement of igneous sills and laccoliths.

NUMERICAL MODELLING

Method

The aim of these numerical models is to investigate shear damage and failure of the host rock of igneous sills emplaced in the Earth's brittle crust. This entails evaluating the static mechanical stability of the brittle overburden of an overpressurized sill. A suitable tool for this problem is limit analysis, which is a standard engineering tool commonly applied to assess the stability of slopes, rock masses and buildings (Sokolovski 1960). The principle of limit analysis is to predict approximate values of loads that bring a brittle solid to an imminent state of failure (Haug *et al.* 2017; Haug *et al.* 2018). Limit analysis is based on two theorems, the lower and upper bound theorems, also called collapse load theorems. The lower bound theorem states that failure will not occur if, for a prescribed set of loads, an equilibrium stress field can be found such that the brittle solid is everywhere below yield. Thus, the lower bound theorem can be used to find the highest prescribed load where no failure occurs. The upper bound theorem states that failure must occur if, for a prescribed set of loads, the rate of working of the external forces on the brittle solid equals or exceeds the rate of internal energy dissipation during failure (Davis and Selvadurai 2005; Krabbenhoft *et al.* 2005). The upper bound theorem can therefore be used to find the lowest prescribed load that still allows failure. This implies that the actual critical load leading to failure of a brittle solid is in between the loads calculated from the lower bound and upper bound theorems. If the range between load estimates calculated from the lower and upper bound is small, the actual critical load that leads to failure is well constrained.

In this study, we apply limit analysis to constrain the critical pressure within a sill that is required to trigger failure of the brittle overburden. The model considers a sill represented by an elongated pressurized cavity of radius R, already emplaced at a depth H in a homogeneous and isotropic Mohr-Coulomb host rock of density ρ, cohesion C and angle of friction ϕ (Figure 7); the sill thickness is set constant at 50 m. To investigate the failure conditions of the sill's overburden, we use the limit analysis software Optum G2 (Krabbenhøft and Lyamin 2014). The

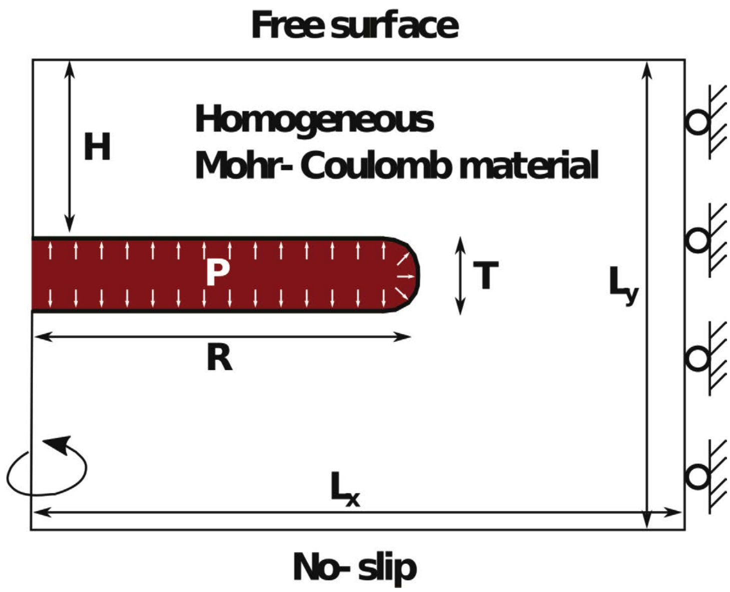

Figure 7. Sketch of limit analysis model setup. The system considered consists of an elongated cavity exerting a homogeneous pressure within a homogeneous and isotropic Mohr-Coulomb material. The system is in an axi-symmetric setting with a free surface at the top, free slip on the right, and no slip at the bottom boundary. From Haug *et al.* (2017).

entire numerical domain is 25 km wide and 8 km high. The system is solved using an adaptive grid with approximately 10000 elements in an axi-symmetric setting (see Krabbenhøft and Lyamin 2014 for more details). We use a free surface on the upper boundary, a semi free-slip condition is applied to the right boundary (Figure 7). At the lower boundary, a no slip condition is used. Several tests have been run using different sill tip shapes, domain sizes and boundary conditions, which have all been documented to produce negligible effects.

Here, we present results from varying geometrical parameters and host rock properties: The host rock cohesion is varied from 2.5 MPa to 100 MPa (Schellart 2000 and references therein), the angle of internal friction is varied from 15° to 60°, and the sill's radius is varied from 250 m to 10 000 m (Haug *et al.* 2018). The density of the host rock is set to 2500 kg/m^3 and the depth of emplacement is varied from 500 m to 4000 m. For each set of parameters, the results of the calculations are (1) both the lower and upper bound solutions of the critical pressure Pc required for brittle failure of the sill's overburden and (2) the resulting distribution of energy dissipation, which we will refer to as "damage".

The assumptions of our models are the following. The mechanical effect of magma within the sill is treated as a homogeneous pressure, such that magma flow and magma density are not accounted for. Further, the critical pressures estimated from limit analysis are calculated for complete collapse of the system, and any propagation of the damage is ignored. The limit analysis formulation considers static systems, as the aim is to investigate the conditions for failure of the overburden of a sill of a given geometry. Thus we assume that the considered sill is emplaced, and we do not consider any host rock damage occurring during the early emplacement of the sill.

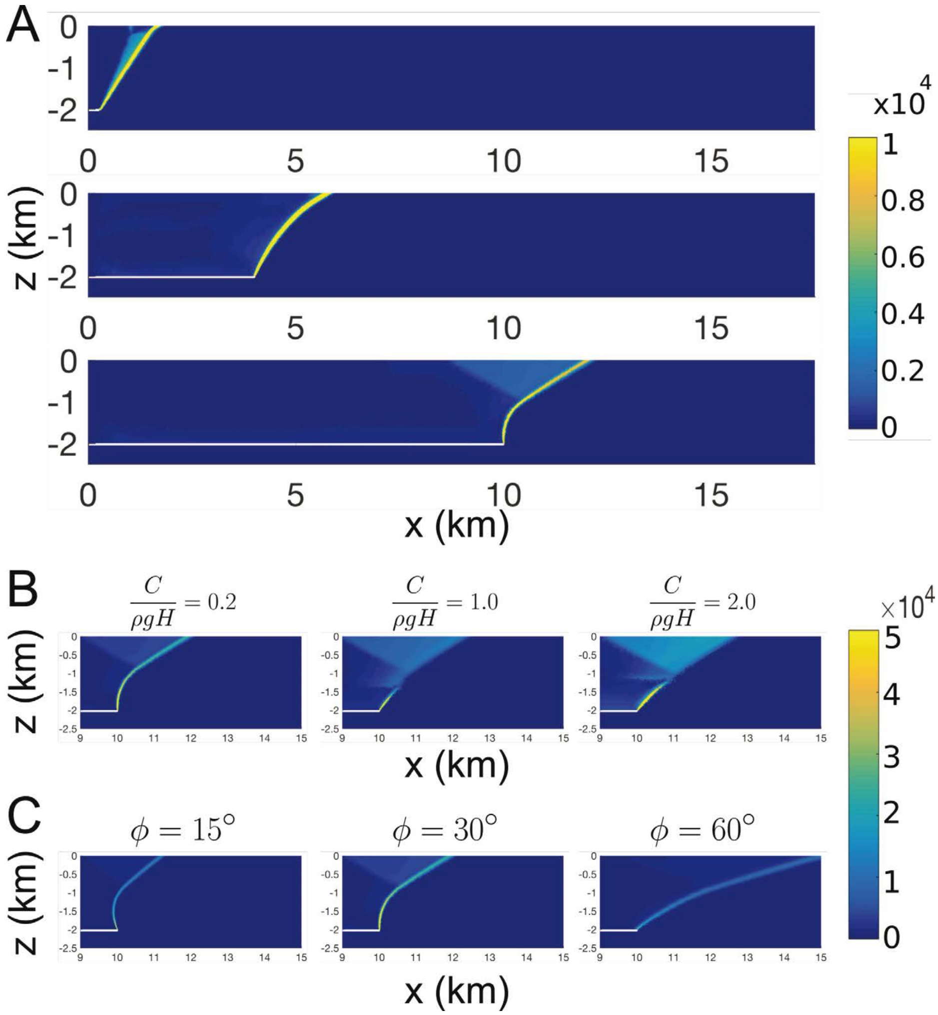

Figure 8. A. Cross sections maps of damage distribution from three models with varying values of R/H. Upper: R/H=0.05. Middle: R/H=2. Bottom: R/H = 5. The other parameters are kept constant (C/(ρgH) = 0.2, Φ = 30°). The horizontal white lines locate the considered sill. The color scale represents the energy dissipated by damage (in kJ), which shows a localization from the tip of the sill towards the surface. B. Cross sections maps of damage distribution from three models with varying values of C/ρgH. The other parameters are kept constant (Φ = 30°, R/H = 5). C. Cross sections maps of damage distribution from three models with varying values of Φ. The other parameters are kept constant (C/ρgH = 0.2, R/H = 2). In both A and B, the color scale represents the energy dissipated by damage (in kJ). From Haug *et al.* (2018).

This assumption implies that the earlier emplacement of the considered sill was associated with limited damage.

Results

In all the simulations, i.e. for all sill diameters, shear damage in the overburden localizes in inclined bands from the sill tip towards the free surface (Figure 8). However, significant differences are observed in the damage distribution depending on the sill diameter (Figure 8). Sills of small diameters (Figure 8A, top) display straight damage zones from the sill tips toward the surface. Intermediate diameter sills (Figure 8A, middle) lead to a gently curved damage band. For sills of large diameters (Figure 8A, bottom), the damage zones consist of steeply-dipping shear zones near the sill tip curving toward gently-dipping outer shear zones near the surface. Haug *et al.* (2017) shows that the damage bands are straight and curved for sills of diameters smaller and greater than 4 km, respectively, the transition between the straight and curved damage bands being quite sharp.

The distribution of damage for changing C/(ρgH)-ratios are presented in Figure 8B, where R/H = 5 and ϕ = 30°. For C/(ρgH)=0.2 the damage zones resemble those in Figure 8A with damage concentrated from the sill tip all the way up to the surface (Figure 8B, left panel). Note that such features are common for all simulations with lower values of C/(ρgH). Conversely, for C/(ρgH)=1 and 2, the sharp concentrated damage zones are observed to no longer reach the surface (Figure 8B, middle and right panel). Instead, it appears to die out some distance away from the tip, and a triangle of distributed damage is observed above it. We will see later that such transition occurs only in models with values of C/(ρgH) larger than a critical value CC of about 0.4.

Figure 8C shows that the distribution of damage is significantly affected by the angle of friction ϕ. Note that the value of C/(ρgH) = 0.2 in the three models displayed in Figure 8C is below the critical value CC mentioned in the former paragraph, such that the models calculate damage across the entire sill overburden. At low angle of friction (ϕ = 15°, i.e. that of weak shale), the damage zone appears as a steeply dipping curved line (Figure 8C, left), while it is less curved and more gently dipping for an intermediate friction angle (ϕ = 30°; Figure 8C, middle). At a high angle of friction (ϕ = 60°, i.e. that of intact granite), the damage zone is gently dipping from the sill tip towards the surface (Figure 8C, right).

IMPLICATIONS FOR HYDROCARBON EXPLORATION

Both our laboratory and numerical models highlight that complex damage and fault patterns can accommodate the emplacement of igneous intrusions, depending on the intrusion shapes and overburden rheology. For instance, our models show that thin sills are associated with small amplitude, localized damage, whereas thick punched laccoliths are associated with numerous, high offset faults through the whole overburden. Our models are thus essential for revealing the structural patterns in the vicinity of igneous intrusions of distinct shapes, which are commonly very challenging to image on seismic data (Figure 4; Delpino *et al.* 2014; Schmiedel *et al.* 2017b; Rabbel *et al.* 2018). Understanding these structures is crucial for enhancing fluid flow modelling around intrusions in order to assess whether these structures are good fluid traps or not. For example, small amplitude forced folds associated with thin sills appear to be very poorly fractured, and so are likely excellent structural traps, such as in the El Trapial field in the Neuquén Basin (Orchuela *et al.* 2003). Conversely, the dome structures above thick, punched laccoliths have the potential to either destroy regional seals like evaporite and shale formations, or connect source rocks to reservoir formations.

Our models are the first able to address the inelastic damage and fracture patterns accommodating the emplacement of igneous intrusions in sedimentary sequences. In particular, they show that even thin sills can trigger significant inelastic damage, and so potential fluid pathways. These results thus bring essential new geomechanical insights with respect to classic elastic models of magma emplacement (Pollard and Johnson 1973; Michaut 2011), which only address the overburden as purely elastic bending solids and are unable to model and predict the inelastic damage and fractures observed in the field. We are aware, however, that our models lack geologically relevant features. For example, our models are homogeneous whereas sedimentary sequences are mechanically layered, which might greatly influence the geomechanical behaviour of the overburden. We will build on these very encouraging results to implement mechanical layering that account for units of different mechanical properties.

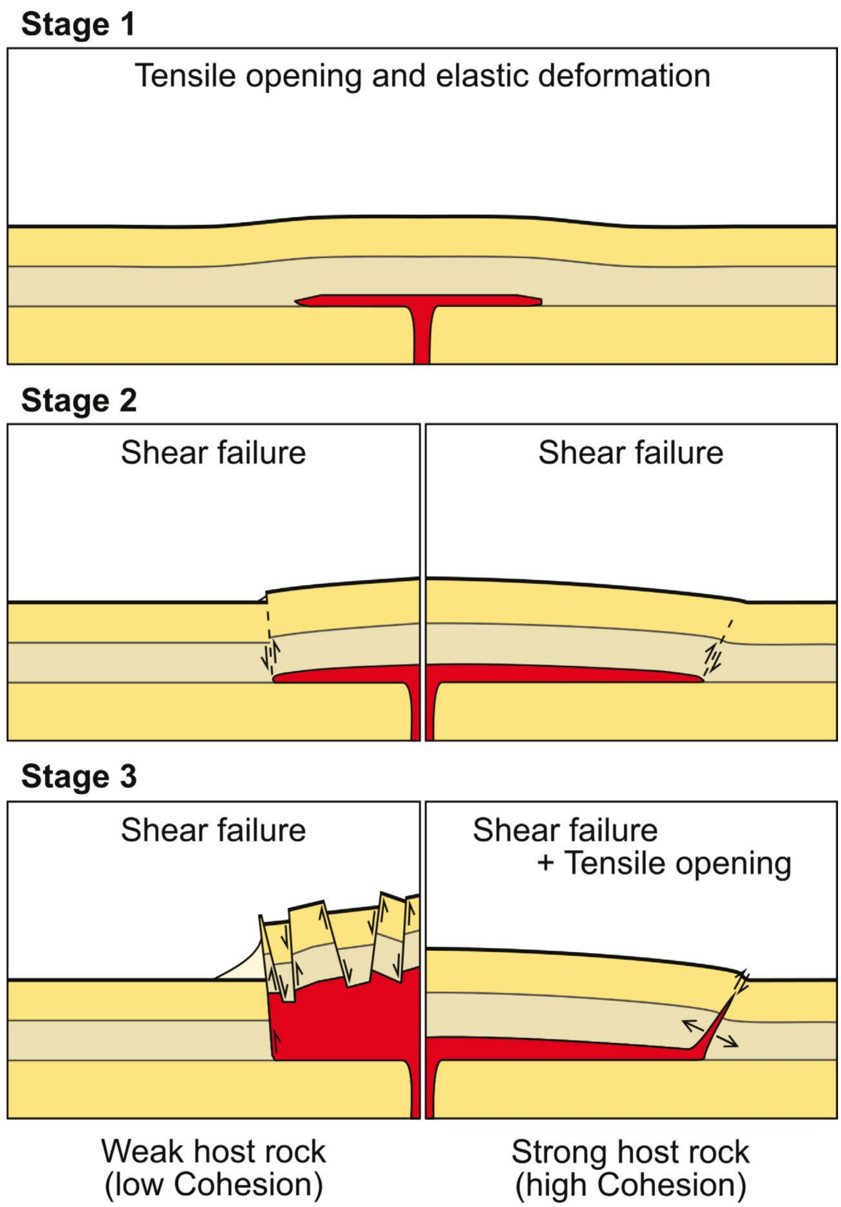

Figure 9. Schematic drawing of the two-stage evolution for horizontal igneous intrusions depending on the failure mode of the host rock. Left: scenario for a low cohesion overburden. Right: scenario for a higher cohesion overburden. From Schmiedel *et al.* (in review).

The models presented in this contribution are purely geomechanical, and intend to address the structural patterns accommodating the emplacement of igneous intrusions in sedimentary sequences. However, we are aware that igneous intrusions also have tremendous thermal impacts, notably when they are emplaced in the source rock. For example in northern the Neuquén Basin, several studies show that the source rock maturation in producing hydrocarbon fields has been dominantly triggered by the heat brought by sill-complexes or laccoliths, which are themselves the reservoirs (Rodriguez Monreal *et al.* 2009; Spacapan *et al.* 2018). This shows that combining geomechanical models and thermal models is essential for quantifying the full impacts of igneous intrusions on the petroleum system.

CONCLUDING REMARKS

Our laboratory and numerical results show that the initial emplacement of both thin sills and massive punched laccoliths is governed by the emplacement of an initial sill until shear failure of the overburden occurs (Figure 9) (Schmiedel *et al.* in review). The subsequent emplacement follows two possible scenarios (Figure 9).

1) If the cohesion of the host is high enough, the rock can sustain open fractures along the shear damage zones leading to the formation of inclined sheets. In this case, the expected damage in the overburden is limited and localized (Figures 1 and 9).
2) Conversely, if the cohesion of the host is low, the rock cannot sustain tensile stresses (i.e., no open fractures), and the resulting massive intrusions form by pushing upward the overburden, which deforms by large amount of shear failure. In this case, the expected damage is extensive and complex, and affects the entire overburden of the intrusion (Figures 1 and 9).

All the results of our models highlight that inelastic deformation of the sill's overburden can develop along shear planes all the way from the intrusion tip to the surface (Schmiedel *et al.* in review). The mechanical relevance of our models is supported by the fact that they are the first able to model intrusions of various shapes, i.e. (1) large concordant sills, (2) saucer-shaped sills, (3) V-shaped intrusions, (4) domed laccoliths, and (5) punched laccoliths. Our models therefore spontaneously reproduce the natural complexity of intrusion shapes and associated deformation patterns as illustrated in Figure 1B. Therefore, our models appear particularly suitable to reveal the structures associated with igneous intrusions, in order to assess their implications for hydrocarbon flow and trap.

An important result of our models is that shear damage greatly accommodate the emplacement of sills and laccoliths, as observed in the field in sedimentary basins (Pollard 1973; de Saint-Blanquat *et al.* 2006; Wilson *et al.* 2016; Spacapan *et al.* 2017). This result shows that the brittle

Coulomb properties of sedimentary rocks are of primary relevance for assessing the structures associated with sills (Guldstrand *et al.* 2017a; Haug *et al.* 2017; Schmiedel *et al.* 2017a). This contradicts the established models of sills and laccolith emplacement, which assume that plastic failure is restricted to small process zones at the close vicinity of sill's tips and can be neglected (Bunger and Cruden 2011; Michaut 2011; Kavanagh *et al.* 2015). This assumption implies that intrusions' host rock dominantly deforms by elastic bending, and that negligible damage occurs. Our models show instead that plastic failure and damage is likely not restricted to domains of negligible size but might extend across large parts of the mechanical systems, highlighting the limitation of the established elastic models.

ACKNOWLEDGEMENTS

Haug and Schmiedel's positions are funded by the Faculty of Mathematics and Natural Sciences at the University of Oslo. Souche and Guldstrand's positions are funded by the Research Council of Norway through the DIPS project (grant no. 240467). We thank OptumCE for giving free academic access to OptumG2.

CITED REFERENCES

Aarnes, I., Fristad, K., Planke, S., Svensen, H., 2011. The impact of host-rock composition on devolatilization of sedimentary rocks during contact metamorphism around mafic sheet intrusions. G3 12, Q10019, 10.1029/2011gc003636.

Abdelmalak, M.M., Bulois, C., Mourgues, R., Galland, O., Legland, J.B., Gruber, C., 2016. Description of new dry granular materials of variable cohesion and friction coefficient: Implications for laboratory modelling of the brittle crust. Tectonophysics 684, 39-51, doi: 10.1016/j.tecto.2016.03.003.

Abdelmalak, M.M., Mourgues, R., Galland, O., Bureau, D., 2012. Fracture mode analysis and related surface deformation during dyke intrusion: Results from 2D experimental modelling. Earth Planet. Sci. Lett. 359-360, 93-105, 10.1016/j.epsl.2012.10.008.

Bunger, A.P., Cruden, A.R., 2011. Modeling the growth of laccoliths and large mafic sills: Role of magma body forces. J. Geophys. Res. 116, B02203, 10.1029/2010jb007648.

Chevallier, L., Gibson, L.A., HNhleko, L.O., Woodford, A.C., Nomquphu, W., Kippie, I., 2004. Hydrogeology of fractured-rock aquifers and related ecosystems within the Qoqodala dolerite ring and sill complex, Great Kei catchment, Eastern Cape, Water Res. Com., S. Afr., p. 127.

Davis, R.O., Selvadurai, A.P.S., 2005. Plasticity and Geomechanics. Cambridge, UK, Cambridge University Press.

de Saint-Blanquat, M., Habert, G., Horsman, E., Morgan, S.S., Tikoff, B., Launeau, P., Gleizes, G., 2006. Mechanisms and duration of non-tectonically assisted magma emplacement in the upper crust: The Black Mesa pluton, Henry Mountains, Utah. Tectonophysics 428, 1-31, 10.1016/j.tecto.2006.07.014.

Delaney, P.T., Pollard, D.D., 1981. Deformation of host rocks and flow of magma during growth of Minette dikes and breccia-bearing intrusions near Ship Rock, New Mexico.

Delpino, D., Bermúdez, A., Vitulli, N., Loscerbo, C., 2014. Sistema de petróleo no convencional relacionado con lacolitos eocenos de intraplaca. Área Altiplanicie del Payún, Cuenca Neuquina, I10° Congreso de Exploración y Desarrollo de Hidrocarburos. Argentinean Oil and Gas Institute (IAPG), Mendoza, pp. 223-242.

Galland, O., Bertelsen, H.S., Eide, C.H., Guldstrand, F., Haug, Ø.T., Leanza, H.A., Mair, K., Palma, O., Planke, S., Rabbel, O., Rogers, B.D., Schmiedel, T., Souche, A., Spacapan, J.B., 2018. Storage and transport of magma in the layered crust-Formation of sills and related float-lying intrusions, in: Burchardt, S. (Ed.), Volcanic and Igneous Plumbing Systems. Elsevier, pp. 111-136.

Galland, O., Bertelsen, H.S., Guldstrand, F., Girod, L., Johannessen, R.F., Bjugger, F., Burchardt, S., Mair, K., 2016. Application of open-source photogrammetric software MicMac for monitoring surface deformation in laboratory models. Journal of Geophysical Research: Solid Earth, 10.1002/2015JB012564.

Galland, O., Burchardt, S., Hallot, E., Mourgues, R., Bulois, C., 2014. Dynamics of dikes versus cone sheets in volcanic systems. Journal of Geophysical Research: Solid Earth 119, 6178-6192, doi: 10.1002/2014JB011059.

Galland, O., Cobbold, P.R., Hallot, E., de Bremond d'Ars, J., Delavaud, G., 2006. Use of vegetable oil and silica powder for scale modelling of magmatic intrusion in a deforming brittle crust. Earth and Planetary Science Letters 243, 786-804, doi: 10.1016/j.epsl.2006.01.014.

Galland, O., Planke, S., Neumann, E.-R., Malthe-Sørenssen, A., 2009. Experimental modelling of shallow magma emplacement: Application to saucer-shaped intrusions. Earth and Planetary Science Letters 277, 373-383, doi: 10.1016/j.epsl.2008.11.003.

Galland, O., Scheibert, J., 2013. Analytical model of surface uplift above axisymmetric flat-lying magma intrusions: Implications for sill emplacement and geodesy. J. Volcanol. Geotherm. Res. 253, 114-130, http://dx.doi.org/10.1016/j.jvolgeores.2012.12.006.

Guldstrand, F., Burchardt, S., Hallot, E., Galland, O., 2017a. Dynamics of Surface Deformation Induced by Dikes and Cone Sheets in a Cohesive Coulomb Brittle Crust. Journal of Geophysical Research: Solid Earth, n/a-n/a, 10.1002/2017JB014346.

Guldstrand, F., Burchardt, S., Hallot, E., Galland, O., 2017b. Dynamics of Surface Deformation Induced by Dikes and Cone Sheets in a Cohesive Coulomb Brittle Crust. Journal of Geophysical Research: Solid Earth, 10.1002/2017JB014346.

Haug, Ø.T., Galland, O., Souloumiac, P., Souche, A., Guldstrand, F., Schmiedel, T., 2017. Inelastic damage as a mechanical precursor for the emplacement of saucer-shaped intrusions. Geology 45, 1099-1102, 10.1130/G39361.1.

Haug, Ø.T., Galland, O., Souloumiac, P., Souche, A., Guldstrand, F., Schmiedel, T., Maillot, B., 2018. Shear versus tensile failure mechanisms induced by sill intrusions – Implications for emplacement of conical and saucer-shaped intrusions. J. Geophys. Res. accepted.

Jackson, C.A.L., Schofield, N., Golenkov, B., 2013. Geometry and controls on the development of igneous sill-related forced-folds: a 2D seismic reflection case study from offshore southern Australia. Geol. Soc. Am. Bull. 125, 1874-1890.

Kavanagh, J.L., Boutelier, D., Cruden, A.R., 2015. The mechanics of sill inception, propagation and growth: Experimental evidence for rapid reduction in magmatic overpressure. Earth Planet. Sci. Lett. 421, 117-128, http://dx.doi.org/10.1016/j.epsl.2015.03.038.

Krabbenhøft, K., Lyamin, A.V., 2014. OptumG2.

Krabbenhoft, K., Lyamin, A.V., Hjiaj, M., Sloan, S.W., 2005. A new discontinuous upper bound limit analysis formulation. Int. J. Num. Meth. Engin. 63, 1069-1088.

Magee, C., Briggs, F., Jackson, C.A.L., 2013. Lithological controls on igneous intrusion-induced ground deformation. J. Geol. Soc. London 170, 853-856.

Michaut, C., 2011. Dynamics of magmatic intrusions in the upper crust: Theory and applications to laccoliths on Earth and the Moon. J. Geophys. Res. 116, B05205, 10.1029/2010jb008108.

Orchuela, I., Lara, M.E., Suarez, M., 2003. Productive Large Scale Folding Associated with Igneous Intrusions: El Trapial Field, Neuquen Basin, Argentina, AAPG International Conference, Barcelona, Spain.

Petford, N., McCaffrey, K., 2003. Hydrocarbons in crystalline rocks. Geological Society, London, Special Publications, London.

Pollard, D.D., 1973. Derivation and evaluation of a mechanical model for sheet intrusions. Tectonophysics 19, 233-269, http://dx.doi.org/10.1016/0040-1951(73)90021-8.

Pollard, D.D., Johnson, A.M., 1973. Mechanics of growth of some laccolithic intrusions in the Henry Mountains, Utah, II. Bending and failure of overburden layers and sill formation. Tectonophysics 18, 311-354.

Rabbel, O., Galland, O., Mair, K., Lecomte, I., Senger, K., Spacapan, J.B., Manceda, R., 2018. From field analogues to realistic seismic modelling: a case study of an oil-producing andesitic sill complex in the Neuquén Basin, Argentina. J. Geol. Soc. London, 10.1144/jgs2017-116.

Rateau, R., Schofield, N., Smith, M., 2013. The potential role of igneous intrusions on hydrocarbon migration, West of Shetland. Petroleum Geoscience 19, 259-272, 10.1144/petgeo2012-035.

Rodriguez Monreal, F., Villar, H.J., Baudino, R., Delpino, D., Zencich, S., 2009. Modeling an atypical petroleum system: A case study of hydrocarbon generation, migration and accumulation related to igneous intrusions in the Neuquén Basin, Argentina. Mar. Pet. Geol. 26, 590-605, http://dx.doi.org/10.1016/j.marpetgeo.2009.01.005.

Schellart, W.P., 2000. Shear test results for cohesion and friction coefficients for different materials: scaling implications for their usage in analogue modelling. Tectonophysics 324, 1-16.

Schmiedel, T., Galland, O., Breitkreuz, C., 2017a. Dynamics of sill and laccolith emplacement in the brittle crust: role of host rock strength and deformation mode. Journal of Geophysical Research: Solid Earth 122, 8625-9484, 10.1002/2017JB014468.

Schmiedel, T., Galland, O., Haug, Ø.T., Breitkreuz, C., in review. Coulomb failure of Earth's brittle crust controls the growth, emplacement and shapes of igneous sills, saucer-shaped sills and laccoliths. Earth Planet. Sci. Lett.

Schmiedel, T., Kjoberg, S., Planke, S., Magee, C., Galland, O., Schofield, N., Jackson, C.A.-L., Jerram, D.A., 2017b. Mechanisms of overburden deformation associated with the emplacement of the Tulipan sill, mid-Norwegian margin. Interpretation 5, SK23-SK38, 10.1190/int-2016-0155.1.

Schutter, S.R., 2003. Occurrences of hydrocarbons in and around igneous rocks. Geol. Soc. London. Spec. Pub. 214, 35-68, 10.1144/gsl.sp.2003.214.01.03.

Senger, K., Buckley, S.J., Chevallier, L., Fagereng, Å., Galland, O., Kurz, T., K., O., Planke, S., Tveranger, J., 2015. Fracturing of doleritic intrusions and associated contact zones: insights from the Eastern Cape, South Africa. J. Afr. Earth Sci. 102, 70-85.

Senger, K., Millett, J., Planke, S., Ogata, K., Eide, C.H., Festøy, M., Galland, O., Jerram, D.A., 2017. Effects of igneous intrusions on the petroleum system: a review. First Break 35, 47-56, 10.3997/1365-2397.2017011.

Sokolovski, V.V., 1960. Statics of Soil Media (translated from Russian by D.H. Jones and A.N. Schofield)). Butterworth, London.

Spacapan, J.B., Galland, O., Leanza, H.A., Planke, S., 2017. Igneous sill and finger emplacement mechanism in shale-dominated formations: a field study at Cuesta del Chihuido, Neuquén Basin, Argentina. J. Geol. Soc. London 174, 422-433, 10.1144/jgs2016-056.

Spacapan, J.B., Palma, O., Galland, O., Manceda, R., Rocha, E., D'Odorico, A., Leanza, H.A., 2018. Thermal impact of igneous sill complexes on organic-rich formations and the generation of a petroleum system: case study in the Neuquén Basin, Argentina. Mar. Pet. Geol. 91, 519-531, https://doi.org/10.1016/j.marpetgeo.2018.01.018.

Trude, J., Cartwright, J., Davies, R.J., Smallwood, J., 2003. New technique for dating igneous sills. Geology 31, 813-816.

Wilson, P.I.R., McCaffrey, K.J.W., Wilson, R.W., Jarvis, I., Holdsworth, R.E., 2016. Deformation structures associated with the Trachyte Mesa intrusion, Henry Mountains, Utah: Implications for sill and laccolith emplacement mechanisms. J. Struct. Geol. 87, 30-46, http://dx.doi.org/10.1016/j.jsg.2016.04.001.

Witte, J., Bonora, M., Carbone, C., Oncken, O., 2012. Fracture evolution in oil-producing sills of the Rio Grande Valley, northern Neuquén Basin, Argentina. AAPG Bull. 96, 1253-1277, 10.1306/10181110152.